



UNIVERSITY OF LEEDS

This is a repository copy of *Nanoparticle-Assisted Water-Flooding in Berea Sandstones*.

White Rose Research Online URL for this paper:

<http://eprints.whiterose.ac.uk/100845/>

Version: Accepted Version

Article:

Hu, Z, Azmi, SM, Raza, G et al. (2 more authors) (2016) Nanoparticle-Assisted Water-Flooding in Berea Sandstones. *Energy and Fuels*, 30 (4). pp. 2791-2804. ISSN 0887-0624

<https://doi.org/10.1021/acs.energyfuels.6b00051>

© 2016, American Chemical Society. This document is the Accepted Manuscript version of a Published Work that appeared in final form in *Energy and Fuels*, copyright © American Chemical Society after peer review and technical editing by the publisher. To access the final edited and published work see <http://dx.doi.org/10.1021/acs.energyfuels.6b00051>.

Reuse

Unless indicated otherwise, fulltext items are protected by copyright with all rights reserved. The copyright exception in section 29 of the Copyright, Designs and Patents Act 1988 allows the making of a single copy solely for the purpose of non-commercial research or private study within the limits of fair dealing. The publisher or other rights-holder may allow further reproduction and re-use of this version - refer to the White Rose Research Online record for this item. Where records identify the publisher as the copyright holder, users can verify any specific terms of use on the publisher's website.

Takedown

If you consider content in White Rose Research Online to be in breach of UK law, please notify us by emailing eprints@whiterose.ac.uk including the URL of the record and the reason for the withdrawal request.



eprints@whiterose.ac.uk
<https://eprints.whiterose.ac.uk/>

Nanoparticle-assisted water-flooding in Berea sandstones

Zhongliang Hu,¹ Siddeequah M. Azmi,² Raza Ghulam,¹ Paul W.J. Glover,² Dongsheng Wen,^{*1}

¹School of Chemical and Process Engineering, University of Leeds, Leeds, LS2 9JT, UK

²School of Earth and Environment Science, University of Leeds, Leeds, LS2 9JT, UK

ABSTRACT: The use of nanoparticles (NP) to improve reservoir characterisation or to enhance oil recovery (EOR) has recently received intensive interest; however there are still many un-resolved questions. This work reports a systematic study of the effect of rutile TiO₂ nanoparticle-assisted brine flooding. Rutile ellipsoid TiO₂ nanoparticles were synthesised and stabilised by tri-sodium citrate dehydrate for brine flooding of water-wet Berea sandstone cores. Careful characterisation of the rock samples and nanomaterials before and after the flooding was conducted, and the relative contributions to the modified flooding results from the stabiliser and the nanoparticles of different concentrations were examined. The oil recovery performance was evaluated both at break-through (BT) point and at the end of flooding (~3.2 pore volumes). Nanoparticle migration behavior was also investigated in order to understand the potential mechanisms for oil recovery. The results showed that both nanoparticle transport rate and EOR effect were strongly dependent on the particle concentration. The oil recovery efficiency at the BT point was found to increase at low nanoparticle concentrations but decrease at higher values. A maximum 33% increase of the recovery factor was observed at the BT point for a TiO₂ concentration of 20 ppm, but higher nanoparticle concentrations usually had higher ultimate recovery factors. The presence of oil phase was found to accelerate the particle migration through the core. The discussion of various mechanisms suggested that the improvement in the mobility ratio, possible wettability change and log-jamming effect were responsible for the observed phenomena.

Keywords: enhanced oil recovery, nanoparticles, water flooding, particle migration, porous medium

1. INTRODUCTION

Various predictions have shown that our demand for oil and gas will still increase in the coming decades. The era of finding “easy oil” is coming to an end, and future supply will become more reliant on fossil fuels produced from non-conventional reservoirs and from enhanced oil recovery (EOR) processes. It is estimated that the average oil recovery rate from mature oilfields around the world is typically 20%-40% of the original oil in place (OOIP) ¹, which leaves enormous potential for developing efficient EOR technologies. Among various secondary or tertiary recovery techniques, water injection is the most-widely used. However, water cannot completely sweep the oil reservoir due to its lower viscosity compared to that of the oil phase ², and a typical microscopic displacement efficiency only reaches 70% or less, due to the capillary trapping of oil in pore space.

Recently, the injection of nanoparticles (NP) has been proposed as a potential means to improve reservoir characterisation and to increase oil production, resulting in the term of NanoEOR ³⁻⁵. Compared to conventional EOR techniques, NanoEOR possesses a few advantages. It is thought that the small particle sizes (<100 nm) would allow them to pass through pore throats of a reservoir rock and be delivered to the locations of the pore network where they can make an active and significant difference in some way. The addition or deposition of different nanoparticles could modify the displacing fluid's effective properties such as viscosity ⁶⁻⁸, interfacial tension ^{9, 10}, and dielectric properties ¹¹; change the permeability of the rock matrix ¹²; or alter the rock surface wettability ^{10, 13}. In addition, the size-dependent properties (i.e., optical, magnetic, electrical, thermo-physical and interfacial properties) of nanoparticles can be used as sensitive down-hole sensors to target locations that are inaccessible by conventional methods ^{5, 14, 15}.

The use of nanoparticles for EOR has received intensive attention since 2008, and much work has been conducted that can be generally categorised as, (i) the development of ‘contrast-agent’ type of NPs to improve the detection limitation of seismic and electromagnetic (EM) techniques and to provide

better reservoir characterisation ¹⁴⁻¹⁶; (ii) the use of NPs as property modifiers, i.e., to alter rock wettability and interfacial tension at the oil/water interface in order to increase oil recovery rate ^{9, 10, 13, 17}; and (iii) the use of NPs for conformance control such as nanoparticle-stabilised emulsions, and gelation materials to block easy flow paths ^{18, 19}.

Following an explosion of hype and speculation, it is beginning to see some advances. However it has to be admitted that the research in this field is just at the beginning. Most of the studies are at the laboratory scale ²⁰ and many contradictory results have been reported, especially regarding the effect of nanoparticles on EOR. For instance, Hendraningrat et al.²¹ showed that the maximum oil recovery was increased by 14.29% of OOIP by using SiO₂ nanoparticles, whereas Bayat et al. ⁴ observed only a 2% increase over OOIP for tertiary oil recovery for the same nanoparticles.

It has been noted that some stabilisers (either surfactants or dispersants) were generally used to stabilise nanoparticles in water or brine, but their characterisation and effects on the oil recovery have seldom been considered ^{22, 23}. These stabilisers alone could significantly affect effective fluid properties especially viscosity and interfacial tension ^{24, 25}, thus having an EOR effect themselves. Consequently it is unclear if the observed effect has been due to the stabilisers, the nanoparticles, or a combination of both.

The stability of nanoparticles in highly saline brines still presents a technical challenge due to the compression of electrical double layer ²⁶⁻²⁸. Learning from the experience of nanofluids ²⁹⁻³³, the displacing fluid's properties will be significantly affected by the choice of nanoparticle material, particle concentration, morphology and stability in salinity water. When applying NPs for oil recovery purpose, such information however was not usually provided sufficiently in literature ²¹, which further hinders interpretation of results.

Multiple possible mechanisms have been proposed to explain the effect of nanoparticles on EOR, including: (i) viscosity increase for mobility control ³⁴, (ii) substrate wettability change ^{9, 10, 13, 17}, (iii) the effect of structural disjoining pressure ^{17, 35, 36}, (iv) the reduction of the displacing fluid/oil

interfacial tension^{9, 10, 37, 38}, and (v) the log-jamming effect^{3, 39}. However none of them have been found to provide sufficient explanation for the observed EOR enhancements. For instance, for the structural disjoining pressure to be effective, a very high nanoparticle concentration is required (>30% by volume⁴⁰). Consequently, it is difficult to invoke this mechanism to explain the results of most published work because these have utilised very small particle concentrations (i.e., in the ppm range).

For NanoEOR to work, another essential aspect that needs to be considered is the effectiveness of nanoparticle migration in rocks. Though extensive work has been conducted on colloidal transport for environmental considerations⁴¹⁻⁴⁴, the transport of nanoparticles in porous media in the presence of oil phase has been scarcely investigated to date. From practical considerations, it is more preferable to use nanoparticles during the secondary water flooding process instead of the tertiary stage, which however has seldom been reported.

A systematic study of the effect of rutile TiO₂ nanoparticle assisted EOR in a sandstone rock is reported in this work. To address the current limitations discussed above, both rock samples and nanomaterials were carefully characterised, including nanoparticle stability in fluids of different salinity. Individual experiments were performed by core-flooding with brine alone (BF), brine with stabiliser (BSF), and with a stabilised suspension of nanofluids in brine (i.e., brine + stabiliser + nanoparticles) (NF), to clearly identify the contributions from the stabiliser and the nanoparticles. The nanoparticle concentrations before and after flooding experiments were determined, and the effects of stabiliser and nanoparticle concentration on the mobility and EOR effect during the secondary water flooding were assessed, as well as an in-depth discussion of the possible mechanisms.

2 MATERIALS, CHARACTERISATION AND FLOODING EXPERIMENTS

2.1 The materials

Synthetic brine (nominally 0.1 mol/dm³ NaCl in deionised water, laboratory grade) was used as the formation liquid and the base fluid for dispersing nanoparticles in all experiments. The density of brine

was measured as $1.000 \pm 0.001 \text{ g/cm}^3$, pH 6.72 ± 0.2 and dynamic viscosity $0.89 \pm 0.01 \text{ mPa}\cdot\text{s}$ at $25 \text{ }^\circ\text{C}$. The oil phase was HVI 60 mineral oil, a highly refined mineral oil that consists of saturated aliphatic and alicyclic hydrocarbons, which has a density of 0.868 g/cm^3 and a dynamic viscosity of $42.75 \pm 0.16 \text{ mPa}\cdot\text{s}$ at $25 \text{ }^\circ\text{C}$. It is less volatile and consequently has physical properties that are more stable than oils of greater volatility, allowing more reliable data to be produced over longer experiments.

There is the potential for confusing concentration of the suspension brine with concentration of nanoparticles in the brine. Consequently, throughout this work we use only the word ‘salinity’ to describe the strength of the brine in which the nanoparticles are suspended and reserve the word ‘concentration’ to denote the amount of nanoparticles per volume of suspension solution.

Titanium dioxide (TiO_2) nanoparticles were synthesised from titanium (III) chloride (TiCl_3) precursors (Sigma Aldrich, UK) using a hydrothermal reaction. Various stabilisers including tri-sodium citrate dehydrate (SCD, Fisher Scientific), sodium dodecyl sulfate (SDS, Fisher Scientific), polyvinylpyrrolidone (PVP, Fluka, Switzerland), polyethylene Glycol 2000 (PEG, Schuchardt, Germany), cetyltrimethylammonium bromide (CTAB, Fisher Scientific), Triton-100 (Sigma Aldrich) and Suwannee river fulvic acid (SRFA, IHSS, USA) were used to stabilise nanoparticles in the brine.

Berea sandstone (Figure 1) is a commonly used clastic reservoir analogue within the hydrocarbon industry. Consequently, its behavior and characteristics are well-known. Berea sandstone is a moderately porous ($\phi \sim 0.18 - 0.25$) sandstone with a high permeability ($k \sim 100 - 1000 \text{ mD}$). It is isotropic and homogeneous, and is composed of well-sorted sub-rounded grains in the range $70 - 400 \text{ }\mu\text{m}$. The grains are predominantly quartz (85 to 90%) and feldspar (3 to 6%) and are cemented by quartz, dolomite (1 to 2%), clays (6 to 8%), and trace amounts of iron sulphides⁴⁵.

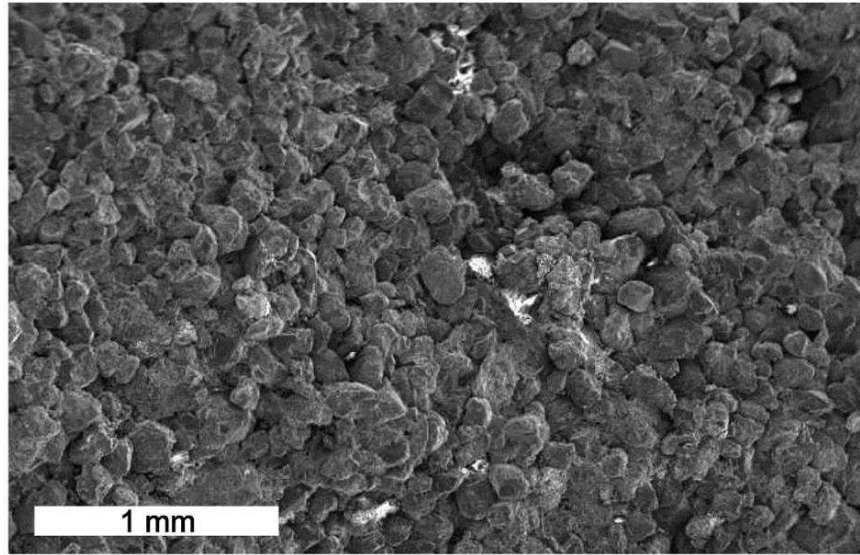


Figure 1. Scanning electron microscope image of a broken surface of the Berea sandstone clearly showing well-sorted sub-rounded grains and a homogeneous and isotropic microstructure.

2.2 Nanofluid fabrication and characterisation

In a typical synthesis, 4.17 cm^3 of 1.5 mol/dm^3 TiCl_3 was added to 250 cm^3 of agitated distilled water. The pH of the system was adjusted to 3.8 ± 0.2 at room temperature by using NaOH and HCl. The solution was stirred by a magnetic stirrer at room temperature overnight for rutile phase synthesis. After the synthesis, extensive dialysis was performed to remove impurities from the NP dispersion.

The morphology of the synthesised particles was examined using a transmission electron microscope (TEM, FEI Tecnai TF20), as shown in Figure 2a. The synthesised nanoparticles were ellipsoidal in shape, with a diameter of approximately $150 \pm 20 \text{ nm}$ and aspect ratio in the range of 7-9. The specific surface area of rutile nanoparticles was determined to be $85.3 \pm 20 \text{ m}^2/\text{g}$ (Acorn AreaTM, XiGo Nanotools Corporate). The hydrodynamic particle size distribution in 0.1 mol/dm^3 NaCl solution (Figure 2b) was measured by a Malvern Nanosizer based on the dynamic light scattering (DLS) method, which shows a distribution between 80-400 nm peaking at $207.7 \pm 14.4 \text{ nm}$. The zeta potential of the dispersion was measured as $-32.0 \pm 1.0 \text{ mV}$.

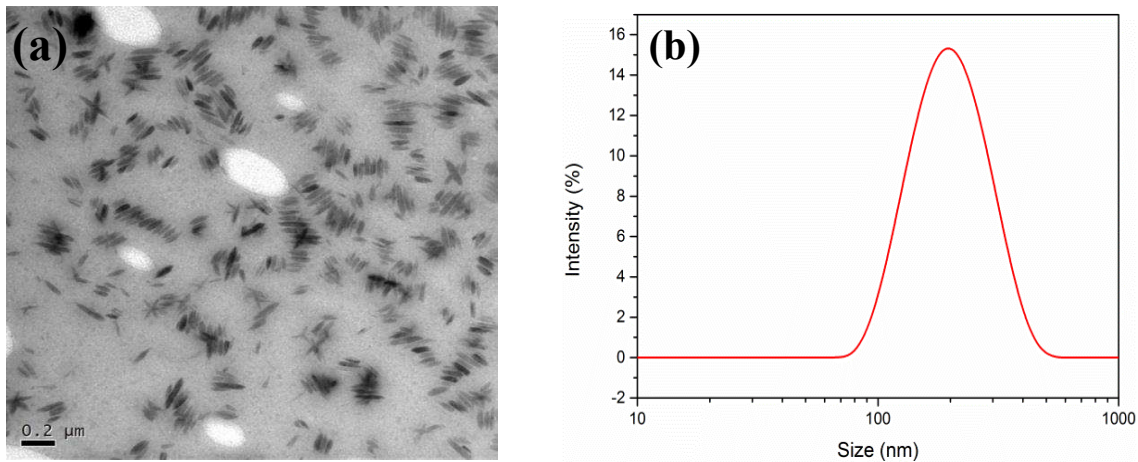


Figure 2. (a) Transmission electron microscope (TEM) images for rutile ellipsoids TiO_2 nanoparticles, and (b) particle size spectrum from the Dynamic Light Scattering (DLS) method.

The effective viscosity was measured using an Anton Paar MCR 301 rheometer at 25 °C and the contact angle and interfacial tensions were measured using a KSV CAM 200 optical tensiometer.

2.3 Core sample preparation and characterisation

A group of water-wet Berea sandstones with permeability ranging from 98.73 mD to 195.46 mD were selected as core plugs in this study. All cores were cleaned by the Soxhlet Extractor method before initial flooding and between each subsequent cycle of flooding. This cleaning procedure used dichloromethane (DCM, or methylene chloride) as the solvent, which is immiscible with water and has a boiling point of 40.1°C. This cleaning process would typically last 7 to 10 days in order to ensure that solvent has extracted all possible oil from the core. Once cleaned by DCM in the Soxhlet Extractor, the cleaned core samples were dried in an oven at 70 °C for 2 days. This cleaning and evacuation process effectively recovered the cores to their initial pre-flooding condition.

The porosity, absolute permeability, and dry core weight were measured for original core samples after each cycle of cleaning in order to verify that the cleaned rocks had similar properties to those of their native states. The dry core weight was measured after 2 days' drying in an oven at 70 °C. The

porosity was determined by both Helium pycnometry and Archimedes (buoyancy) methods. For the Archimedes method, the rock samples were fully saturated with brine, of a known density, in a vacuum desiccator for 4 hours to ensure 100% saturation. The pore volume, grain volume and grain density were calculated from the recorded dry, saturated and suspended masses, as shown in Table 1. As expected, the saturation porosity was slightly smaller than the helium porosity, due to the size, polarity and large molecular weight of water compared to helium. All four cores had similar porosities and pore volume. However there is a moderate variation in the permeability, ranging from 99 -195 mD.

Table 1. Basic rock properties

No.	Length (mm)	Diameter (mm)	Archimedes Method					Helium Method Porosity (%)	Permeability (mD)
			Bulk Volume (cm ³)	Pore Volume (cm ³)	Porosity (%)	Grain Volume (cm ³)	Grain Density (g/cm ³)		
SZ1	65.030	38.018	72.96	13.46	19.0	59.52	2.61	21.20	150.92±0.39
SZ2	64.749	37.922	72.52	13.42	18.0	59.10	2.58	21.08	138.46±0.80
SZ3	65.470	37.886	73.56	13.40	18.0	60.16	2.66	20.82	98.73±0.59
SZ4	66.109	37.884	74.26	13.84	19.0	60.43	2.61	21.01	195.46±0.56

An examination of the morphology of grains and pores in the core samples, as well as an elemental analysis were carried out using scanning electron microscope (SEM, FEI Quanta 650 FEG-ESEM) and integrated energy-dispersive X-ray spectroscopy (EDX, Oxford X-max 80 SDD) with INCA 350 software. It can be seen from Figure 3 that the majority of the pore sizes were above several micrometers, while confirming that the grains were composed of silica (SiO₂) with minor contributions from clays (calcium, iron and aluminum).

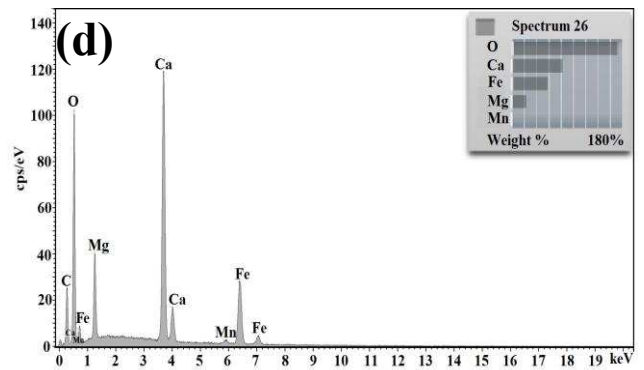
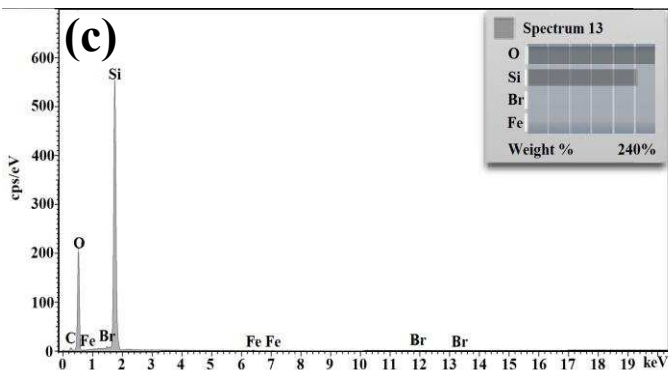
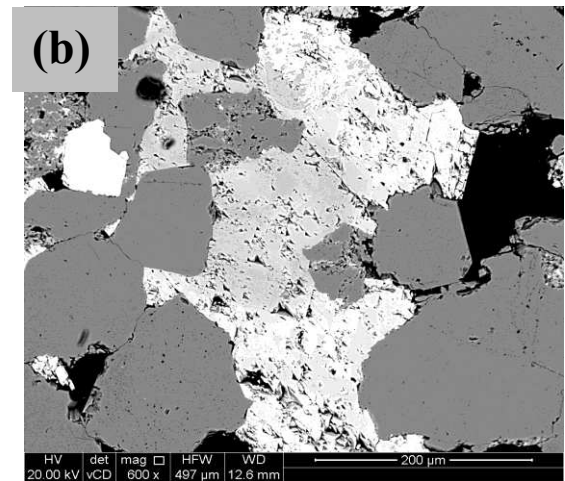
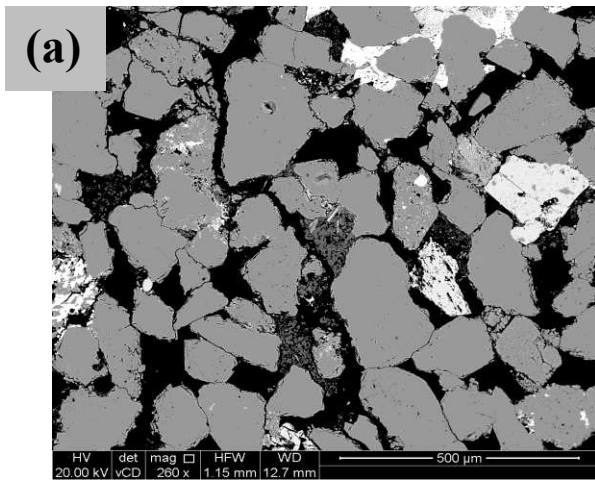


Figure 3. (a) SEM of the Berea sandstone with pores shown in black, silica grains in light gray and feldspar in white; (b) higher magnification SEM image of feldspar and porosity between silica grains; (c) EDX spectrum of sand grain showing peaks only for silicon and oxygen; (d) EDX analysis of feldspars.

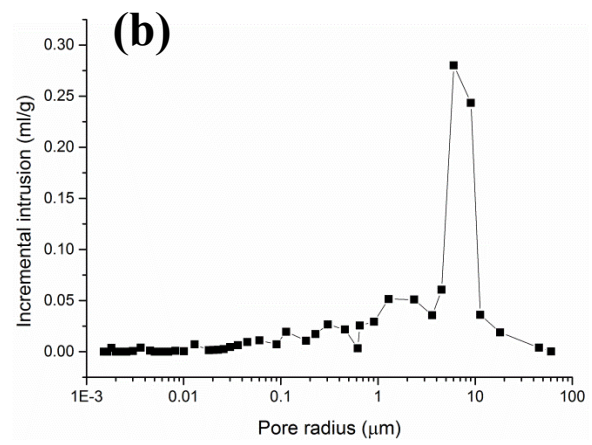
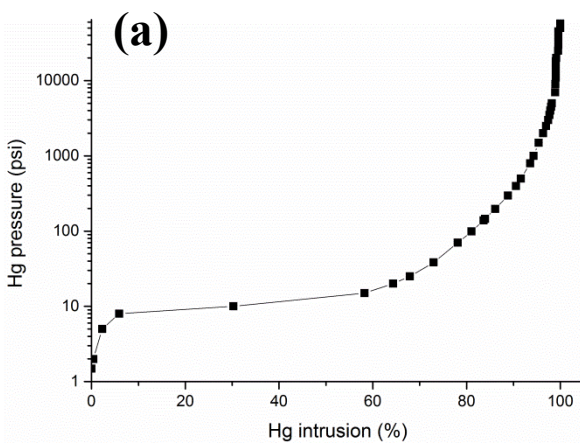


Figure 4. Core sample characterisation by MICP. (a) Mercury injection capillary pressure curve

showing the pressure (y -axis) required to effect a change in mercury saturation in the sample (x -axis).
(b) Inverted pore throat radius spectrum showing a well-defined characteristic pore throat size of 7 – 10 μm .

Mercury Intrusion Capillary Pressure (MICP) was used to determine the pore size distribution. The measurements were conducted on a small piece of Berea sandstone, representing an off-cut from the core plugs used in the flooding experiments. The porosity was 19.7 %, similar to the helium pycnometry values shown in Table 1. The specific pores area from MICP measurements was 1.01 m^2/g . It can be concluded from Figure 4 that 88% of pore throat diameter centralised in the 0.6 - 36.2 μm range, providing a mean diameter of 14.09 μm , with 6% pore throat diameters below 227 nm. This size is very close to the hydrodynamic diameter of the rutile ellipsoids nanoparticles, which implies that a small percentage of pore throats could be blocked by nanoparticles.

2.4 Core flooding experiments

A core flooding system was set up to reveal the nanoparticle-assisted water potential for EOR. Figure 5 shows the integrated experimental instruments and schematic view of the core-flooding setup. A Hassler type core holder, in which the brine-saturated core was loaded, was located vertically and supported by a customised stand. Fluid was injected through the core-holder vertically upwards. Inside the holder, the core was enclosed in an elastic rubber sleeve, upon which was applied a radial overburden pressure of 1500 psi around the rock sample via a high pressure hydraulic hand pump (P142, ENERPAC). The maximum fluid pressure in the experiment was smaller than 500 psi, which ensured that no fluid leakage between the sleeve and the core sample. . An inlet and outlet port in each end plug allowed upstream and downstream flow lines and pressure transducers to be attached. Any brine introduced into the core flooding system was de-aerated in a vacuum pump for 4 hours. The dead volume of the core flooding system was calibrated and all measurements were corrected for it. A back-

pressure regulator was used to raise the pore pressure inside the core during brine saturation stage, to ensure that gas bubbles were completely removed from the core-flooding system at the start of the experiment by dissolution.

To clarify the effect of potential influence of stabilisers, three cycles of water-flooding tests were conducted. Each set of experiments began with a water-flooding with only the synthetic brine (BF) followed by a water-flood with the synthetic brine and the nanoparticle stabiliser but no nanoparticles (BSF), and finally nano-flooding using the synthetic brine, stabiliser and different concentrations of nanoparticles (NF). The cores were cleaned as discussed earlier between each water-flooding cycle.

The experimental procedure for each cycle included the following stages:

- Core sample was fully saturated with brine in a vacuum desiccator for 4 hours to ensure 100% saturation, and then was inserted into core holder;
- Brine saturation at a flow rate of $2 \text{ cm}^3/\text{min}$ for 6 pore volumes (PV);
- Oil saturation at a flow rate of $17 \text{ cm}^3/\text{min}$ until an ‘irreducible’ water saturation of $S_{wi} = 25\%$ was achieved;
- Flooding at a flow rate of $0.5 \text{ cm}^3/\text{min}$ for 3 PV, with the fluid of interest;
- Remove core from core holder. Core cleaning and preparation, ready for the next cycle.

This simulates secondary flooding of the reservoir.

During each flooding experiment, graduated cylinders marked in 0.1 cm^3 divisions were used to collect the effluent sample in order to determine the volume of oil and water. During NF experiment, effluent samples were collected manually during the flooding process and a total of 15-19 effluent samples of 1.5 cm^3 each were analyzed. The nanoparticle size distribution of the effluents was determined off-line by the DLS device, and UV-Vis spectroscopy was used to measure the particle concentration. The determination of concentration was based on the comparison of the effluent absorbance against an established calibration curve between the absorbance and nanoparticle

concentration. The concentration of nanoparticle suspension entering cores, C_0 , and the concentration of sample collected, C , were applied to generate breakthrough curves of C/C_0 as a function of pore volumes passing through the porous medium. Detailed sample characterisation was conducted for nanofluids after the flooding experiments.

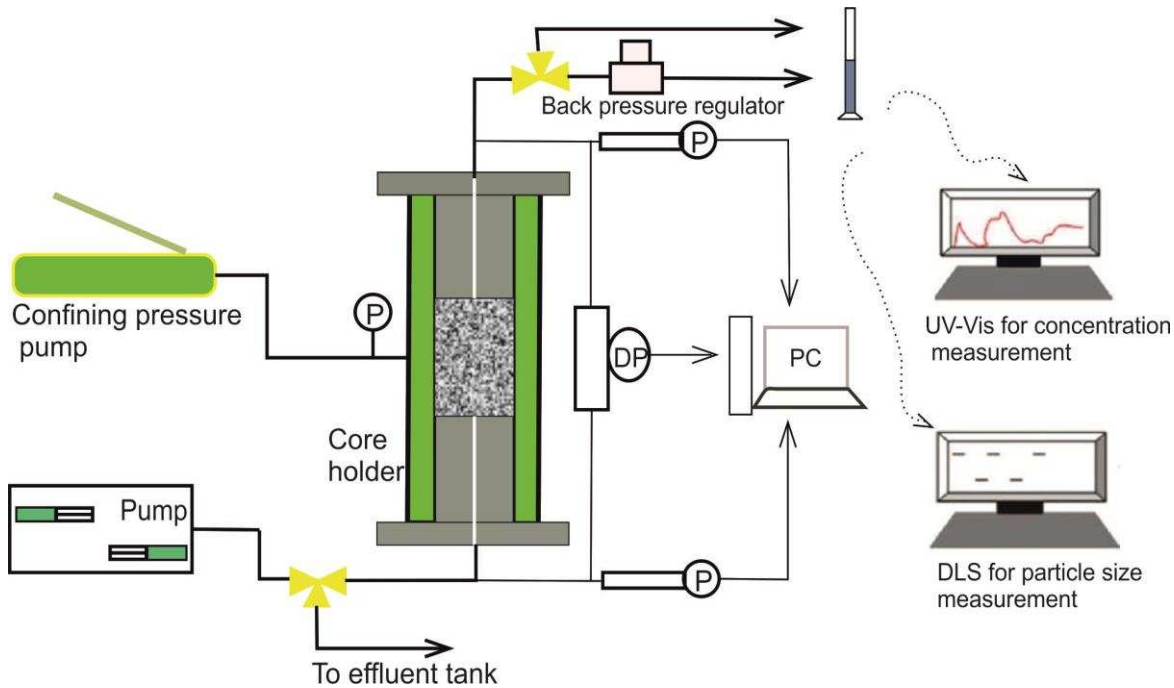


Figure 5. Schematic flow diagram for the flooding system

3 RESULTS AND DISCUSSION

3.1 Nanofluid stability

For any practical application, nanoparticles have to be stabilised properly in the presence of various ions similar to the composition of brine. The stabilisation mechanism could be either steric⁴⁶, electrostatic⁴⁷ or a combination of both. Many researchers have reported that nanoparticles cannot be stabilised easily in high salinity water⁴⁸⁻⁵², especially when the ionic strength exceeds the critical salt concentration (CSC)⁴⁸. The presence of ions, especially divalent cations such as Mg^{2+} , Ca^{2+} and Ba^{2+} , could significantly reduce the stability due to the compression of the electric double layer^{28, 50, 53}.

The agglomeration kinetics of TiO_2 under the influence of a number of stabilisers mentioned earlier were assessed in 0.1 mol/dm^3 and 1 mol/dm^3 NaCl salinity, in order to determine the right stabilising

agent to use. In this exercise, the TiO₂ nanoparticle concentration was 500 ppm and the pH was adjusted to 6.8 ± 0.3 , whilst gentle magnetic stirring was applied. All surfactant concentrations were fixed at 0.3 wt % relative to the water content, except SRFA whose concentration was 100 ppm. The main results are given in Figure 6. Regardless of the stabiliser, an increase in the brine salinity clearly increases particle size (Figure 6a). Tri-sodium citrate dehydrate (SCD) showed the best performance in terms of particle size and was chosen for the following further experiments.

The particle size and zeta potential evolution of four SCD-stabilised nanofluids of different concentrations from 10 ppm to 500 ppm in a 0.1 mol/dm³ NaCl brine were measured over a two week period following their fabrication, as shown in Figure 6b. There was a slight increase in hydrodynamic particle size for almost all concentrations over two weeks, but this always remained lower than 240 nm. Absolute values of zeta potential often saw sharp decreases in the first 4 days, becoming more stable during the remainder of the two week period, at around -27 ± 3 mV for the 50, 100 and 500 ppm concentration samples, and below -18 mV for the 10 ppm sample. Extrapolation implies that the low concentration sample would become stable at about -14 ± 3 mV after about 3 weeks.

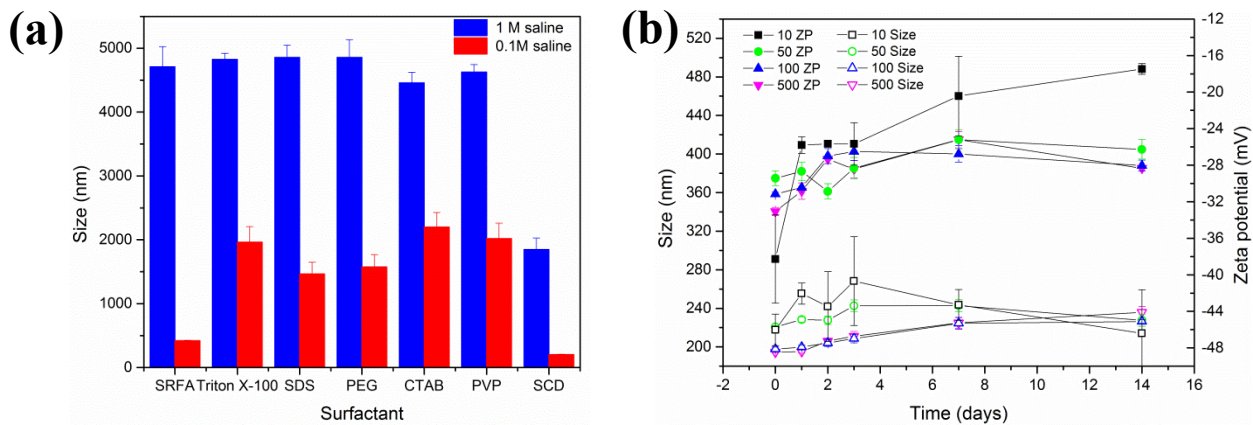


Figure 6. Stability of TiO₂ nanoparticles (rutile ellipsoids), (a) average particle size comparison for different stabilisers and two brine salinities (0.1 mol/dm³ and 1 mol/dm³ NaCl), and (b) temporal behaviour of the average particle size (open symbols) and zeta

potential (solid symbols) for four different TiO₂ nanoparticle concentrations (10, 50, 100 and 500 ppm) in a 0.1 mol/dm³ NaCl brine solution stabilised by SCD)

3.2 Fluid properties

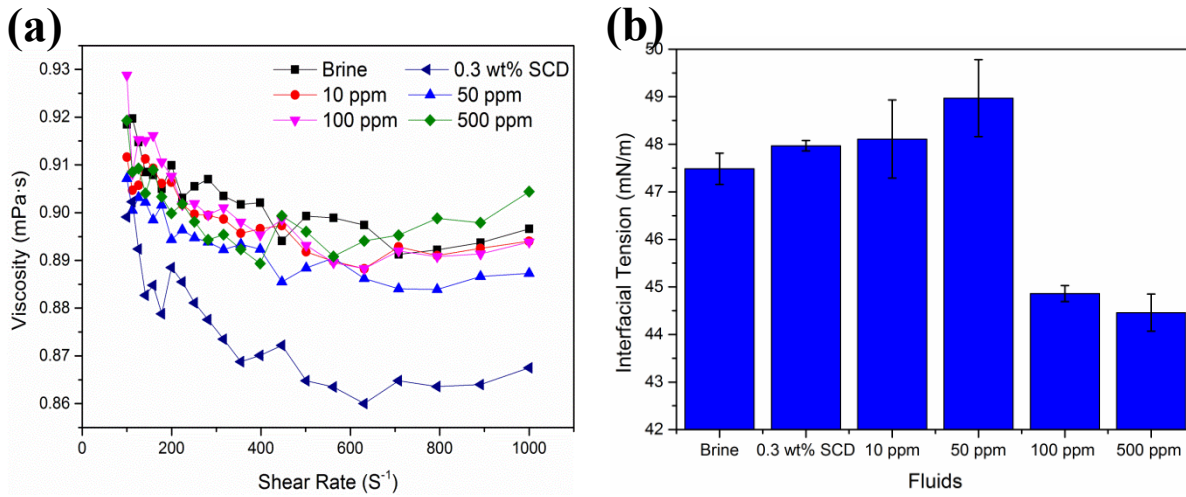


Figure 7. (a) Dynamic viscosity, and (b) interfacial tension of the 0.1 mol/dm³ brine alone, the 0.1 mol/dm³ brine with 0.3 wt % SCD stabiliser, and the stabilised brine with 10, 50, 100 and 500 ppm of TiO₂ nanoparticles.

The dynamic viscosities of the base fluid, base fluid with stabiliser and all four nanofluids are shown in Figure 7a. The dynamic viscosity for the mineral oil was also measured at 41.2 mPa·s. This relatively high dynamic viscosity is beneficial, assisting in reducing the irreducible water saturation S_{wi} to 25% in a water-wetting rock.

The introduction of the stabiliser (SCD) alone reduced the viscosity significantly, but the effective viscosity returned to almost the level of the initial brine after the inclusion of nanoparticles. The effect of particle concentration on the effective dynamic viscosity was therefore small due to the low particle concentration.

The addition of SCD alone slightly increased the interfacial tension (IFT) of the base fluid, as shown in Figure 7b, reaching about 47.97 ± 0.11 mN/m for an SCD concentration of 0.3 wt %. The influence

of nanoparticles on IFT is not monotonic but the variation was small, having a maximum value of 49.0 ± 0.8 mN/m at 50 ppm and a minimum of 44.5 ± 0.4 mN/m at 500 ppm. Such results showed a similar trend with other literature data^{31,40}, where there is extensive study on the influence of nanoparticles on IFT.

3.3 Rock property changes

The absolute permeability and helium porosity were measured after each flooding cycle to track whether the rock itself was damaged or modified by the core-flooding processes. The results are summarised in Figure 8, which show that the change of porosity from core-flood to core-flood was small for all rock samples, with the largest variation in the range of 2% for sample SZ2. Nearly constant porosity was observed for both samples SZ3 and SZ4 during different stages of the flooding.

The permeability experienced a drop after the BF and BSF flooding, but the change was small after the NF flooding. This suggests that the stabiliser used may have a deteriorating effect on the permeability. Some stabilisers may partially remain inside the rock during the flooding and reduce the permeability. In contrast, the nanoparticles do not cause permeability impermeability. Core samples SZ2 and SZ4 showed that the permeability increased slightly after the NF flooding, suggesting that some blockage caused by the stabiliser-only flooding was removed during the NF flooding. This clearly shows the importance of proper selection of stabilisers. As the porosities and absolute permeabilities for all rocks after NF flooding were very close to those after BSF flooding, two of the cleaned rocks (SZ1 and SZ2) were selected for 5 ppm and 20 ppm NF flooding respectively.

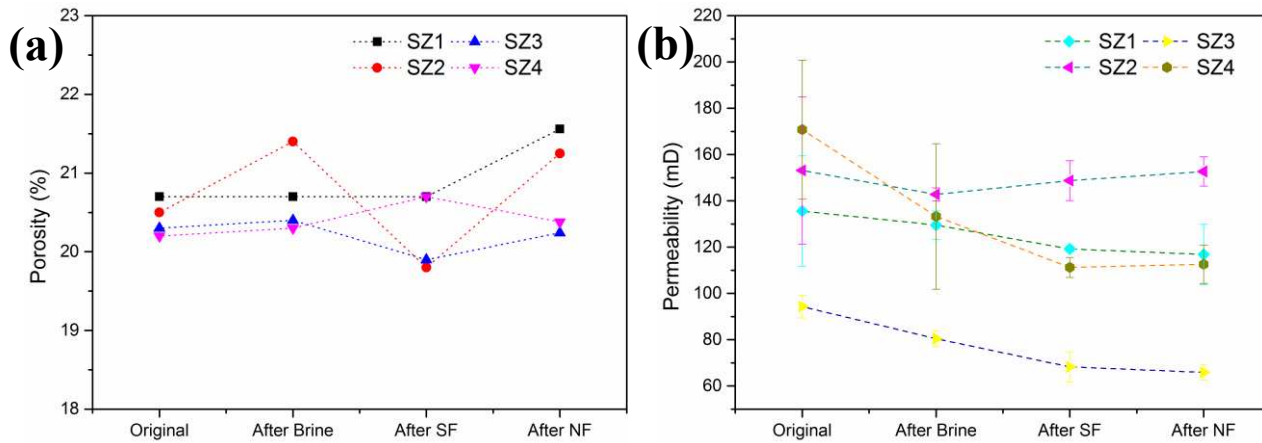


Figure 8. Variations of (a) sample helium porosity, and (b) sample permeability for original core samples, and for the cleaned cores after core-flooding with brine (After Brine), brine and stabiliser (After SF) and nano-flooding (After NF).

3.4 Core-flooding results

While we measured the oil and brine production regularly during each core-flooding (as shown in Figure 9), we paid particular attention to the cumulative oil production, and hence the oil recovery efficiency at three main points of interest: break-through (BT) point, 1PV of displacing fluid injection, and ultimate recovery point. The former value indicates the practical oil recovery amount when the breakthrough occurs, whereas the last one indicates the maximum amount of oil that can be recovered for a given flooding. The breakthrough was usually defined identified as the moment when the first drop of water was produced at the downstream of the core, allowing for a dead volume delay correction. It was observed that additional oil recovery becomes small after about 1 PV and the cumulative oil recovery (COR) was calculated at 3.2 PV, by which time no more oil could be collected for another 20 minutes.

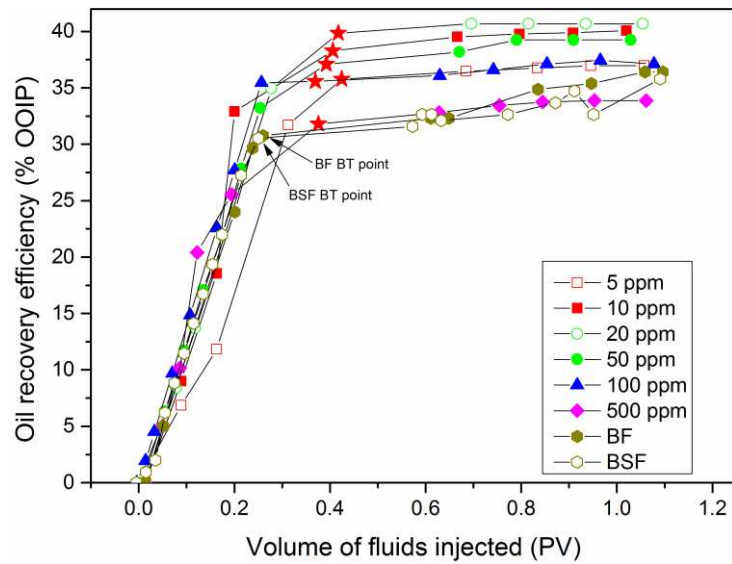


Figure 9. Examples of the volume of oil recovered from 0 to 1 PV expressed as a percentage of the initial oil saturation. The stabiliser is 0.3 wt % SCD, and data is given for synthetic brine (BF), synthetic brine with stabiliser (BSF) and for synthetic brine, stabiliser and six different concentrations of TiO₂ nanoparticles. The breakthrough points are marked by red five-pointed stars.

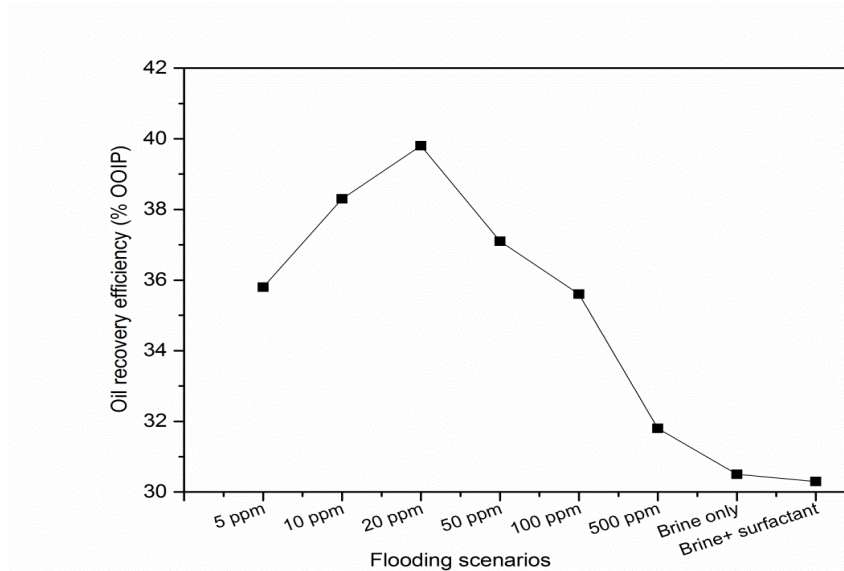


Figure 10. Oil recovery at breakthrough expressed as a percentage of the initial oil saturation for synthetic brine (BF), synthetic brine with stabiliser (BSF) and synthetic brine + stabiliser and six different concentrations of TiO₂ nanoparticles. The stabiliser is 0.3 wt % SCD.

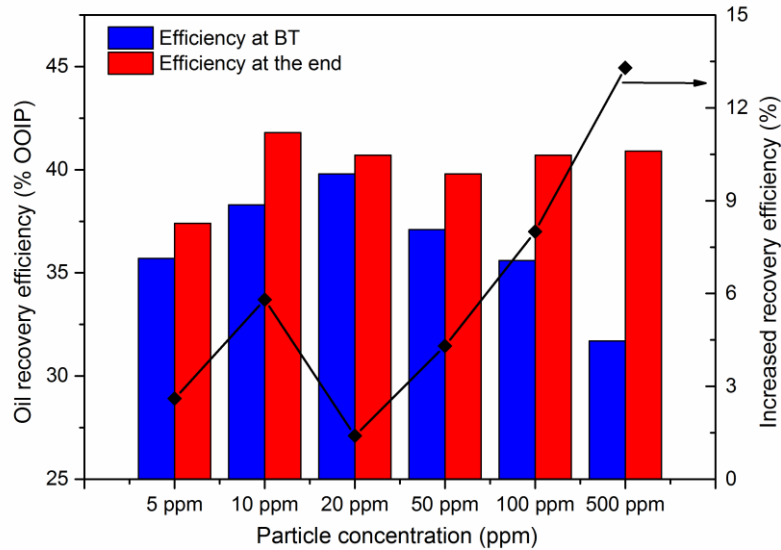


Figure 11. COR at breakthrough (blue bars) and at the end of flooding (red bars) expressed as a percentage of the initial oil saturation for six different concentrations of TiO₂ nanoparticles, together with the amount of oil produced after breakthrough (solid diamonds and lines) expressed as a percentage of the oil in place at breakthrough. The stabiliser is 0.3 wt % SCD.

Figure 9 shows that there was a rapid recovery of oil immediately following the fluid injection and before brine breakthrough. In this part of the core-flooding the aqueous fluid pushes the oil out of the sample in a quasi-piston-like displacement process, and the oil recovery increases approximately linearly with the volume of injected displacing fluids. This linear increase in oil production ends after the injection of about 0.4 PV, when brine breakthrough occurs.

The cumulative oil recovery at breakthrough is shown in Figure 10. The BT point was observed at about 0.25 PV for the brine only (BF) and brine with stabiliser floods (BSF), and in the range of 0.35 to 0.45 for TiO₂ nanofluid floodings (NF) with different concentrations of nanoparticles. Brine only flooding resulted in an average of 30.3% recovery of the oil originally in place (OOIP), and a similar value (i.e., 30.5 %) was found for flooding with a mixture of brine and stabiliser (BSF). This shows that the influence of the 0.3 wt % SCD stabiliser on the oil recovery was negligible in this work.

However it should be noted that this is not a universal conclusion. Other stabilisers especially some designed surfactants, could affect the oil recovery rate significantly, and their effects should be identified appropriately in any experiments to illustrate the nanoparticle effect. Figure 10 clearly shows that adding TiO_2 nanoparticles can increase the oil recovery rate significantly but in a non-linear manner. At lower particle concentrations, the oil recovery rate increases with the increase of particle concentration, reaching a peak value at about 20 ppm, after which it starts to decline. About 35.8 % of the oil originally in place was recovered at the lowest concentration of nanoparticles tested, i.e. 5 ppm, compared to the use of brine only (30.3%). The best oil recovery of the tested scenarios was about 39.8% of OOIP, which occurred for a nanoparticle concentration of 20 ppm. This represents nearly a 31.4% increase in oil recovery compared to water-flooding with plain synthetic brine or brine with stabiliser but no nanoparticles. However, further increase of particle concentration resulted in a decrease in the enhancement of oil recovery compared to the plain brine and brine with stabiliser cases. For a nanoparticle flooding with a concentration of 500 ppm, an oil recovery of only 31.8% of OOIP was achieved at the breakthrough, representing only around 5% enhancement of oil recovery over flooding with brine or brine with stabilisers but no nanoparticles.

The COR at the end of the experiment is shown together with that at breakthrough in Figure 11. The general dependence of the COR on particle concentration was found to be similar to that at breakthrough, but the peak value occurred for a 10 ppm nanofluid, with a total oil recovery of 41.8% of OOIP, representing a 38.0% increase on the plain water-flooding scenario.

Unlike the breakthrough case, there was no substantial decrease in total COR at the end of the experiment for nanofluids with concentrations greater than 20 ppm, instead these fluids progressively exhibited a large post-breakthrough production of oil. Despite having the lowest recovery at breakthrough, the 500 ppm nanofluids achieved a COR at the end of the experiment of 40.9% of OOIP, second only to the total recovery of the 10 ppm nanofluid. The 500 ppm nanofluid mobilised an additional 13.3% of the oil in place at breakthrough point. We have attributed the mechanism for post-

breakthrough enhancement of oil production to ‘log-jamming’ of some pores with nanoparticles which then forces oil to be produced from adjunct pores where it was previously trapped. This mechanism is discussed in the following sections.

3.5 Nanoparticle migration behaviour during flooding

3.5.1 Pressure profiles among different flooding cycles

Examples of three differential pressure profiles that were measured during the different cycles of flooding are shown in Figure 12, for a single core. The nanoparticle concentration in this figure is 500 ppm and occurs in the data represented by blue triangles. The behavior indicated in the figure suggests that a log-jamming effect^{3, 39} may be significant in the core-flooding with the 500 ppm nanofluid.

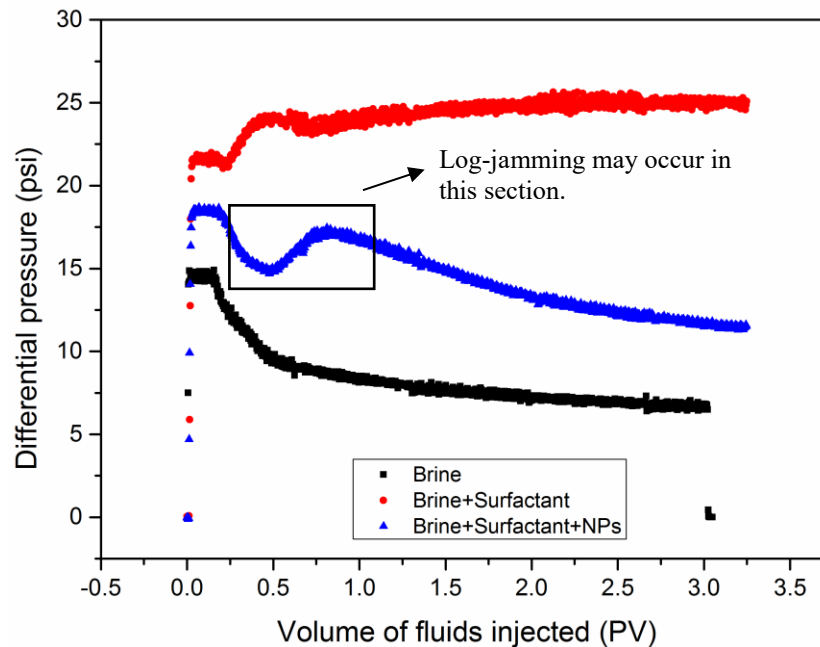


Figure 12. Pressure profiles for brine (black points), brine with stabiliser/surfactant (red points) and a 500 ppm TiO₂ nanofluid (blue points) flooding on core SZ4. The initial pressures should be the same at the start, at which time there is still oil to be introduced by the leading dead-volume. The differential pressure offsets between each of the flooding profiles is caused by small permeability differences between flooding cycles as shown in Figure 8b).

For the brine flooding (BF) the pressure steadily decreases as the oil is removed from the core sample and the permeability within the core increases. For the brine + stabiliser flooding (BSF), despite oil production and the removal of oil from the core, the differential pressure increases. The high pressure drop suggests that the stabiliser in the brine could form micelles or aggregates, and block some pores through the course of the brine flooding, hence reducing the core's permeability, as supported by the permeability measurement in Figure 8b. The trapped stabilizer could not be removed by the following course of the flooding.

The NF flooding showed a higher pressure drop than that of BF but lower than the BSF case. This was due to that most of the stabilizers were on the surface of particles, and the quantity of loose stabilizer in the brine was small, hence reducing the possibility of stabilizer jamming. In addition, during the flooding process, nanoparticles also tended to mobilise or assist in the migration of loose stabilisers stuck in the core samples and mobilized the residual oil. Such effects would result in a higher permeability and a lower differential pressure profile than the BSF case. The increase in differential pressure for the nanofluid flooding, as highlighted in Figure 12, suggests that a portion of the nanoparticles became temporarily stuck in the core, reducing the permeability, and increasing the differential pressure. Subsequent decrease of pressure, after 0.8 PV, may be caused by the un-blockage of the jammed particles. It is thought that the accumulation of nanoparticles at the entrance of pore throats would produce a higher pressure in the adjunct pore channel, in which the oil trapped would be mobilised. Similar observations have been reported by a few previous studies^{3, 39}. The presence of oil phase may promote the jamming effect as the nanoparticles were diffused to the oil-water interfaces and were confined there, consistent with the enriching of particle concentration at the oil/water interface phenomenon, as identified by a few prior studies⁵⁴⁻⁵⁶.

3.5.2 Nanoparticle breakthrough behaviour

Ultra-violet spectrophotometer measurements have been used to monitor the amount of nanoparticles transported through the core samples. The measurement is based on absorbance and can be affected by the morphology of particle in the fluid. The presence of salt tends to form aggregates, leading to a large absorbency increase and a higher than unity C/C_o value, as evidenced for the 10 ppm case, Figure 13.

Figure 13 shows that nanoparticle transport is strongly dependent on the nanoparticle concentration. The outlet to inlet concentration ratio, C/C_o , generally decreases with increasing particle concentration. For example, for a 10 ppm nanoparticle concentration, breakthrough was achieved quickly with C/C_o approaching unity at 0.43 PV just as the first drop of nanofluid emerged from the core. The 50 ppm nanoparticle sample showed a similar early breakthrough at 0.39 PV but with a reduced concentration of nanoparticles in the emerging fluid ($C/C_o = 0.7$), implying that up to 30% of the injected nanoparticles remained within the core. At higher nanofluid concentrations (100 ppm and 500 ppm) the concentration of nanoparticles in the breakthrough fluid is even less ($C/C_o = 0.65$ and $C/C_o = 0.18$, respectively) with more of the injected nanoparticles remaining inside the core (Figure 13). The peak concentration for the 500 ppm nanofluid flood was reached at 1.69 PV, and the maximum transport ability stayed below 20% (i.e., $C/C_o < 0.2$).

Each flooding experiment was followed by an injection of a further 4 PV of plain synthetic brine in order to check if the particles were strongly stuck inside the rock. This brine post-flooding process was conducted after the end of the nanofluid flooding at 3.2 PV for all experiments. The results (i.e., right-most part of Figure 13) show that significant amounts of NPs can be cleaned out from the cores immediately following the brine flooding. However after another about 3 PV of brine, no more nanoparticles can be driven out, suggesting that some nanoparticles remain trapped in the cores.

Further calculation shows that, for the highest concentration (500 ppm) flooding, 19.66 mg of nanoparticles in total (87.2% of the total injected amount) were deposited in the rock during nanofluid

flooding and remained trapped there, which corresponds to about 17.15 mg of TiO₂ nanoparticle per square meter of grain surface, which represents an coverage of 0.92% of the rock's internal surface area if it is assumed that the nanoparticles are deposited as a monolayer (Table 2).

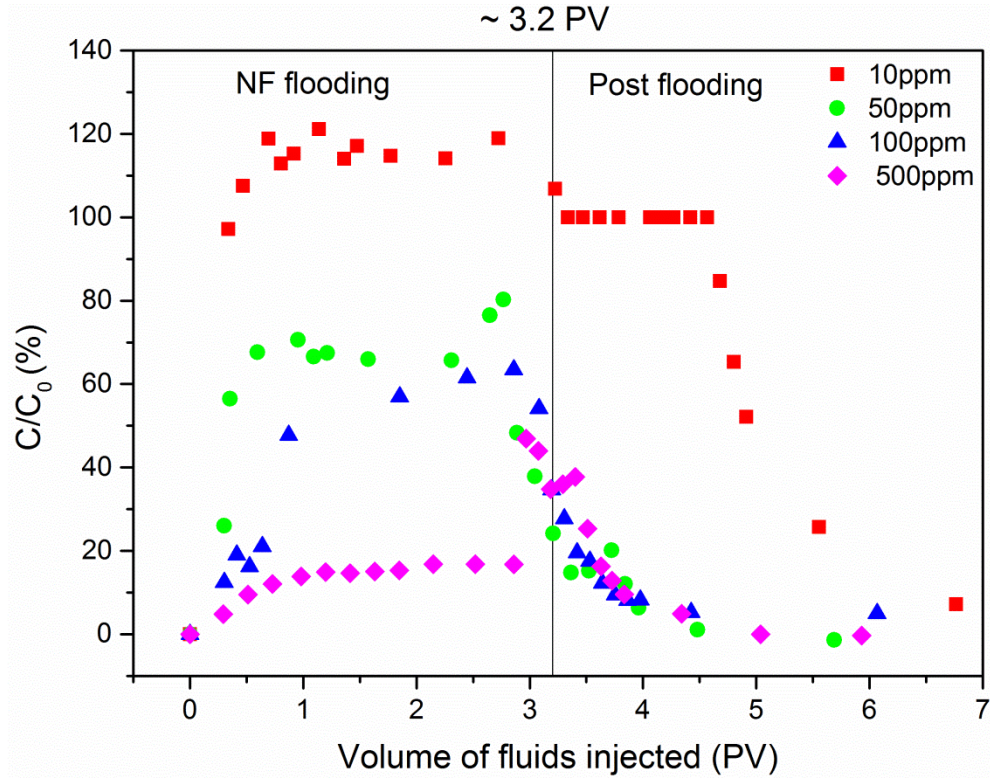


Figure 13. Particle breakthrough ability during flooding with four different concentrations of TiO₂ nanofluid and subsequent post-flooding with synthetic brine. C₀ is the concentration of initial fluids before NF flooding.

Table 2. Nanoparticle retained in core samples during nanofluid flooding.

Rock No.	NP conc. (ppm)	Total NP mass (mg)	NP mass retained in core (mg)	NP retained in core (%)	Total internal pore surface area (m ²)	Mean retained NP trapping density (mg/m ²)	Mean area of internal pre surface coated (%)
SZ1	10	0.375	-0.133	NA	154.73	NA	NA
SZ2	50	1.685	0.776	46.0	152.58	0.005	0.08
SZ3	100	3.786	2.248	59.4	157.26	0.014	0.22
SZ4	500	19.659	17.152	87.2	158.32	0.108	0.92

Fine particle migration in porous medium is an area of extensive research interest^{41,42}. It is known that the mobility of particles is affected by four main mechanisms; (i) blockage, (ii) adsorption, (iii) straining, and (iv) gravity sedimentation. The adsorption effect would be small in this study because our nanoparticles are negatively charged, and the zeta potential of Berea sandstone is negative at high ionic strength⁵⁷ and in the range of pHs encountered in these experiments and in hydrocarbon reservoirs^{28,58,59}. The gravity sedimentation effect is also expected to be small due to short residence time of particles in the core and the effect of Brownian motion.

In this work, it appears that the particle migration was affected mostly by pore-throat blockage and straining (i.e., a log-jamming effect), as well as the presence of oil phase. The blockage effect is highly dependent on the particle concentration⁶⁰. This is supported by SEM and MICP analysis of the Berea sandstone (Figure 1 and Figure 3), the latter of which shows that around 6% of pore throats are under 220 nm when subjected to quantitative image analysis, i.e., less than the hydrodynamic diameter of nanoparticle (Figure 2). These relative dimensions suggest strongly that the blockage could take place, especially when the fluid contains high concentrations of nanoparticles. Consequently, log-jamming of larger pore throats with high concentrations of nanoparticles is consistent not only with the relative dimensions of the pores and nanoparticles themselves, but also with the data shown in Figure 12 and Figure 13, making it an important factor influencing particle migration and implying that high nanoparticle concentrations should be avoided in NanoEOR.

In order to examine the NP migration behaviour without the presence of oil, 100 ppm nanofluids were injected into Berea sandstone directly after brine saturation. The comparative results (Figure 14) show that the nanoparticles present a faster breakthrough in the presence of oil. Significant amount of nanoparticles were detected at the exit of the core sample at about 0.8 PV in the presence of oil, but their presence was delayed to about 1.5 PV in the absence of the oil phase. The Berea sandstone used in this work is strongly water-wet. Consequently, the water phase occupies the pore spaces close to the grain surfaces and the oil phase occupies discrete drops or connected ganglia in the centre of pores,

which are continuous through pore throats when they are sufficiently wide and can modify the electrical and hydraulic connectedness of the fluids in the pores ⁶¹.

The transport of the nanoparticles is confined to the aqueous phase because the rutile ellipsoids TiO_2 nanoparticles used in this work are water-wet. The early breakthrough for the transport of nanoparticles in the presence of oil exhibited in Figure 14 occurs because the nanoparticles are confined to be transported in the water phase that initially occupies only a fraction of the pore volume. Consequently any given volume of injected nanofluids, expressed in pore volumes, will displace more than its apparent volume of water phase and hence apparently travelling through the core more efficiently. That same nanofluid is also displacing oil, which is produced, so that the injection of nanofluids becomes apparently less and less effective as the nanofluid flooding progresses, explaining why the data for the displacement in the presence of oil appears to start effectively with a breakthrough at about 0.5 PV, but becomes less efficient after about 1.4 PV. By contrast, in the absence of an oil phase the nanofluids have the entire pore volume to travel through during the entire injection process. The breakthrough is consequently delayed until about 1.2 PV.

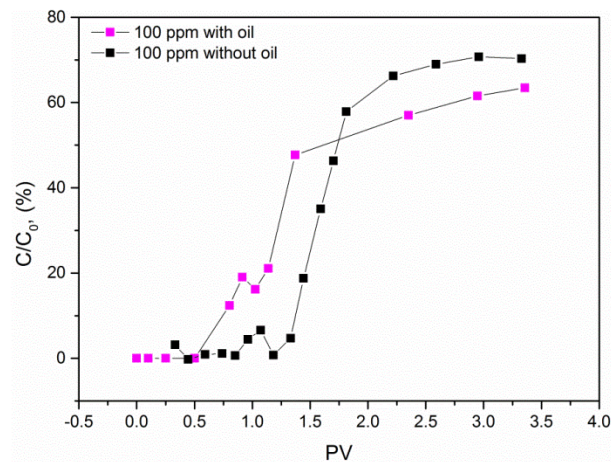


Figure 14. Nanoparticle transport during core-flooding with a 100 ppm concentration nanofluid with and without presence of oil. The ratio of the concentration of nanoparticles at the outlet to that of the inlet (C/C_0) is shown as a function of pore volumes of nanofluid injected.

3.5.3 Particle size distribution

The particle size distribution of the effluent samples was examined by the dynamic light scattering (DLS) method. It was interesting to observe that the hydrodynamic size of the effluent nanoparticles showed a bimodal distribution, which has also been reported by previous studies¹⁶. Consequently, although the size distribution of the injected samples show a monomodal range of about 100 nm to 400 nm (Figure 2b), the effluent samples exhibit a population of nanoparticles in the range 10 nm to 100 nm and a larger group, ranging from about 100 nm to 400 nm. It is clear that passage through the rock has effectively separated the two size fractions.

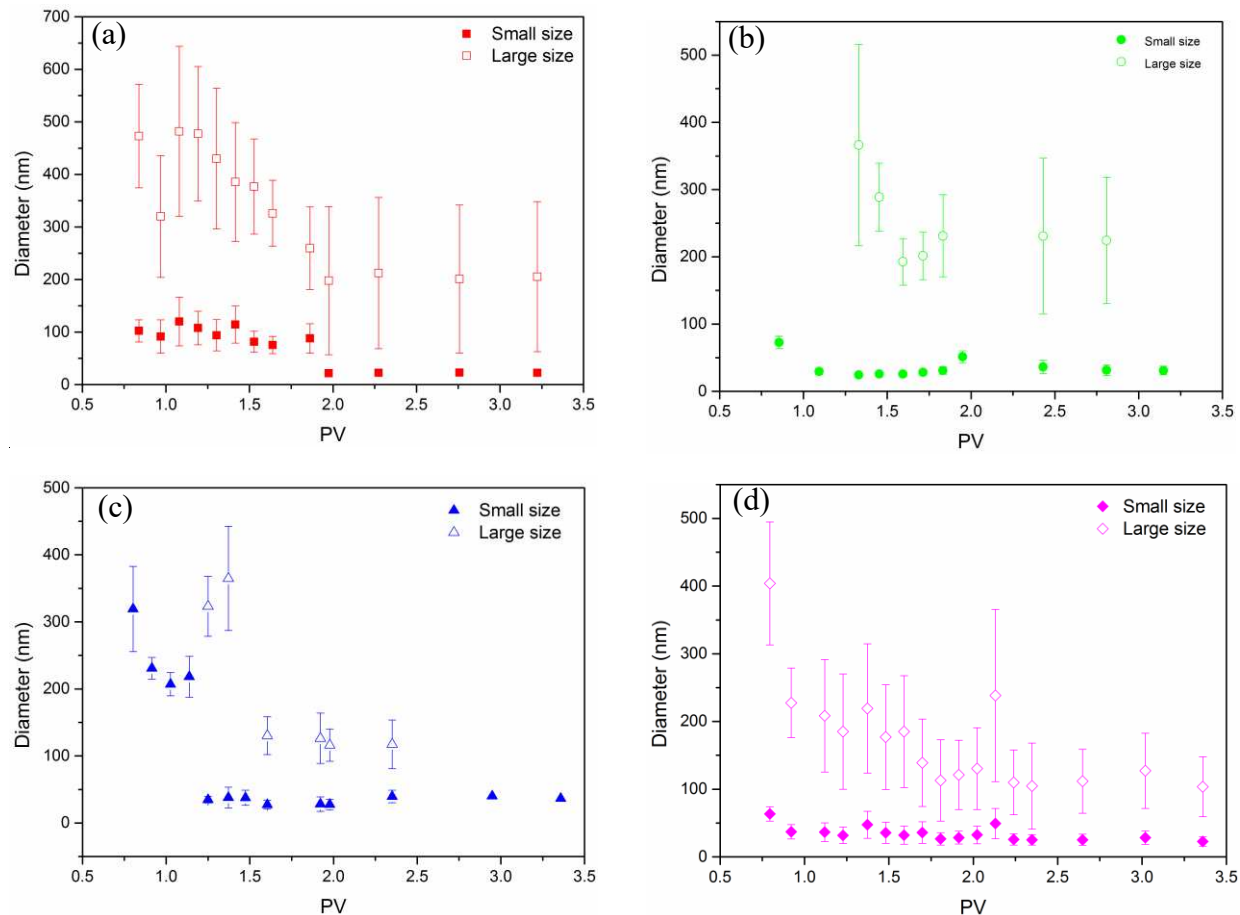


Figure 15. Effluent nanoparticle size distributions for nanofluid core-flooding with different nanoparticle concentrations; (a) 10 ppm, (b) 50 ppm, (c) 100 ppm, (d) 500 ppm.

The peak particle sizes of the two modes and a measurement of their ranges at different flooding volumes are shown in Figure 15. It is interesting to note that the smaller and larger fractions of

nanoparticle occur in the effluent, but the middle range does not. This implies that it is the nanoparticles of intermediate size that become trapped in the cores, suggesting that the choice of nanoparticle size is a critical one for designing an efficient NanoEOR process.

As discussed above, a few particle migration mechanisms were responsible for the particle mobility, and among those, the log-jamming effect could form large loose agglomerates, responsible for the forming of the large particle population. It is also interesting to note that for all nanoparticle flooding scenarios, the particle size for the larger population of nanoparticles decreased from around 300 nm to around 100 nm as the flood progressed (Figure 15).

3.6 NanoEOR mechanisms

The results in this paper so far clearly show that well-stabilised nanofluids can increase oil recovery, and that the effect is strongly dependent on the nanoparticle concentration. A nearly 33% increase of oil recovery at breakthrough has gone beyond our initial expectation. As reviewed briefly in the introduction section, many potential mechanisms have been proposed for the nanoparticle enhancement of oil recovery, but none are well-accepted yet.

We have seen in Section 3.5 that log-jamming is likely happen after breakthrough, especially for high nanoparticle concentrations, such as 100ppm and 500 ppm in this research, and this may contribute to the enhancement of oil recovery. We will examine other mechanisms in depth here.

3.6.1 The effect of mobility ratio modification

The mobility ratio is generally defined as the mobility of the displacing phase divided by the mobility of the displaced phase, which can be expressed by equation (1)⁶²

$$M = \frac{k_{rw}}{\mu_w} / \frac{k_{ro}}{\mu_o} = \left(\frac{k_{rw}}{k_{ro}} \right) \left(\frac{\mu_o}{\mu_w} \right), \quad (1)$$

where k_r is the relative permeability, μ refers to dynamic viscosity, the subscript w represents displacing phase (usually water), and the subscript o is for the displaced phase (usually oil). The ratio shows the mobility of the injecting fluid to that of the oil phase, and the effect is dependent on the

relative permeability and the viscosity ratio. The value of M was larger than unity in this work, indicating higher water mobility than that of the oil. Under these conditions the displacing fluid (brine, brine and stabiliser and nanofluids) would invade the rock through a non-uniform front, resulting in an early breakthrough, which is supported by Figure 9. Clearly, reducing the mobility ratio could lead to a higher oil recovery. Figure 7a shows that the effective viscosity of the nanofluid was almost independent of nanoparticle concentration within the 5 ppm to 500 ppm range used in this work. However, the produced oil (Figure 16) shows a small reduction in viscosity, which we attribute to containing of nanoparticles. It is still unclear about the effect of nanoparticles on relative permeability curves. There have been a few limited studies which show that the inclusion of different nanoparticles could affect the relative permeability ratio significantly¹² and this modification might be through the modification of the wettability of the rock by the deposition of nanoparticles, as will be discussed later in this work.

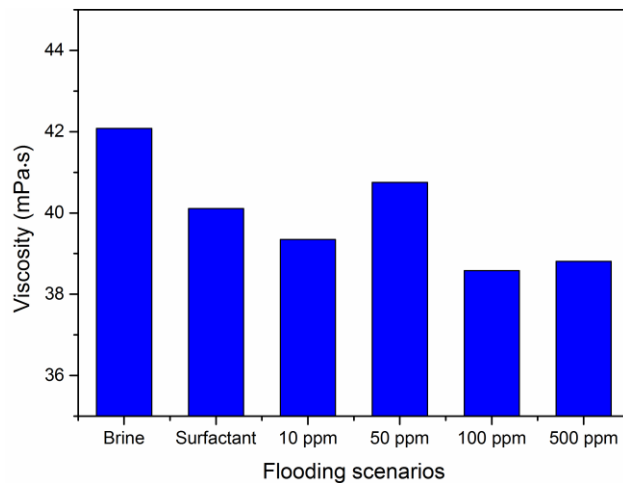


Figure 16. Viscosity of produced oil for synthetic brine (BF), synthetic brine with stabiliser/surfactant (BSF) and for synthetic brine, stabiliser and four different concentrations of TiO_2 nanoparticles.

3.6.2 The capillary effect

One of the proposed mechanisms for NanoEOR requires that nanoparticles reduce the oil/water interfacial tension and consequently improve the oil recovery^{9, 10, 38, 63}. This mechanism is applicable

mainly to the mobilisation of residual oil which is trapped by capillary forces, and is governed by the dimensionless Capillary Number C_a , which shows the relative importance of the viscous force to capillary force,

$$C_a = \frac{\mu_i \times \vartheta}{\sigma}, \quad (2)$$

where μ_i is the dynamic viscosity of injected fluid (Pa·s), ϑ is Darcy's velocity (m/s), σ is the interfacial tension (N/m).

We have already shown that the influence of nanoparticles on the dynamic viscosity and interfacial tension are small in this work (as shown in Figure 7). The calculated Capillary Number is of the order of 10^{-7} , which is too small to increase oil recovery by freeing residual oil. Jeong (2005) suggested that the capillary number should be of the order of 10^{-5} or higher in order to produce a significant enhancement of oil recovery. Clearly the influence of the capillary effect was not, therefore, responsible for the observed NanoEOR effect.

3.6.3 The structural disjoining pressure effect

The structural disjoining pressure (SDP) effect was proposed by Wasan & Nikolov³⁵. The SDP is different from the conventional disjoining pressure, which is a result of the London-Van der Waals force that has a short range. It has been demonstrated that the structural disjoining force is generated from the ordering of nanoparticles in a confined wedge (structuring) and the influence can extend to a film depth of a few nanoparticle diameters (long range)³⁵. The origin of the structural disjoining pressure is due to the confinement of the particles in the film region as opposed to their greater freedom of location in the bulk liquid. The layering arrangement of the particles gives rise to an excess pressure in the film, the structural disjoining pressure, which has an oscillatory decay profile with the film thickness. A result of such a structure force is that nanofluids could exhibit a good spreading capability in confined spaces. Such forces have been observed (i) to be able to change the macroscopic contact

angle of a liquid droplet ⁶⁴⁻⁶⁶, (ii) to stabilise liquid films ⁶⁷, and (iii) to lift an oil droplet from a wall in an aqueous solution ^{36, 68-72}

As shown by ³⁶, the SDP could be important for mobilising individual oil droplets. However as suggested earlier, the droplet form of oil was unlikely in the current experiments. In addition there are two major concerns for such an approach, namely, the concentration effect and the transient effect ⁴⁰. The modelling results of SDP show that the increase in wettability with concentration is non-linear and it only becomes important at high particle volume concentrations (i.e., >20%). However most of NanoEOR experiments reported were based on very dilute nanofluids with typical concentrations of below 1% in weight. The structural disjoining pressure may not be that important although nanoparticles have a tendency to migrate into the microlayer to form ordered solid-like layers. Of note though, as the increase of local concentration, the increased viscous effect could become important and should be considered as well. Another concern is that the modeling was based on the steady state, and only the equilibrium shape of the meniscus under the action of an oscillatory structural disjoining pressure was calculated. Such a model could be only valid during the flooding if the oil displacement time is much longer than that of forming ordered nanoparticle layers.

3.6.4 The surface wettability effect

Nanoparticle deposition and subsequent rock surface wettability modification has been proposed by a few researchers in order to explain the NanoEOR effect. For example, Li et al.¹⁰ found that nanoparticles can change an already water-wet rock surface to a more water-wet surface, while Karimi et al.¹³ found that an oil-wet rock surface can be made to be strongly water-wet by ZrO₂ nanoparticles, leading to a considerable amount of oil recovery. By contrast, Roustaei et al.⁹ have argued that changing the rock surface towards oil-wet could change the role of the capillary force from a barrier to a driving force, which would be beneficial for oil recovery. In addition, several authors ^{17, 63, 73} have

proposed that the main mechanism for NanoEOR is wettability change of rock surface from either water or oil wet to neutral wettability.

In our experiments the Berea sandstone core samples were generally water-wet, but measurements (Figure 17) have indicated that saturation of the sandstone with increasing concentrations of nanoparticles can change it to have an even higher wetness to water, contributing to an increase in the recovery factor.

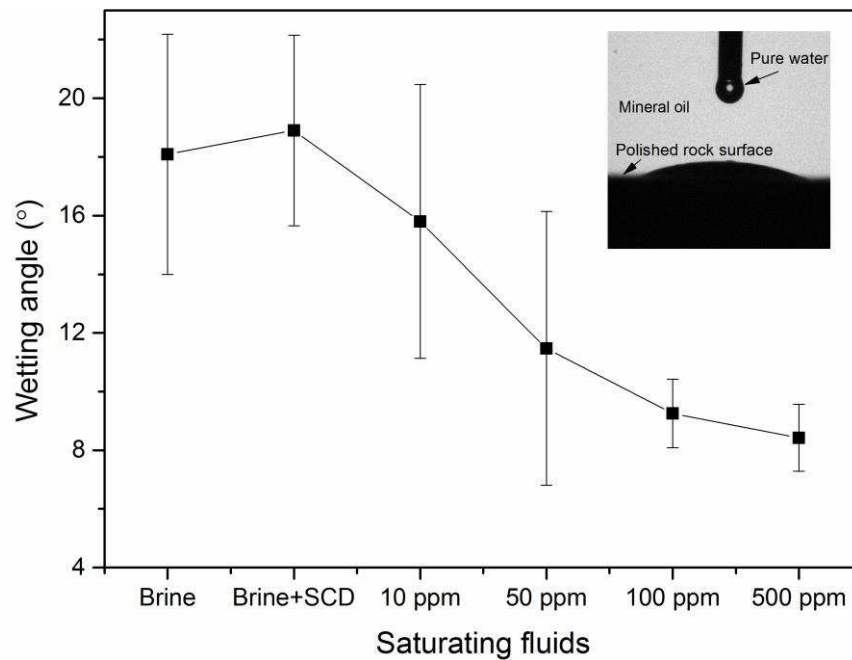


Figure 17. Evaluation of the wetting angle of pure water to Berea sandstone, which were immersed in mineral oil and pre-saturated with varying concentrations of TiO_2 nanoparticles. Inset: an example photograph of one such measurement.

3.6.5 Possible reasons for observed EOR effect

Having examined the known possible mechanisms that could cause the enhancement of oil recovery with nanofluids that is observed in this work, we may say that mobility control, log-jamming and wettability changes may all have a role to play. However, it is difficult to quantify the exact contribution of each. Additional experiments are currently being carried out in order to clarify the contribution of each mechanism.

4 CONCLUSIONS

A systematic study of the effect of rutile TiO₂ nanoparticle assisted brine flooding was conducted in this work. Comprehensive characterisation of the rock sample and nanomaterials before and after the flooding was carried out. The relative EOR contributions from the stabiliser and the nanoparticles have been identified. The effect of using different concentrations of TiO₂ nanoparticles has also been studied. Finally, the known possible mechanisms of nanoparticle-assisted secondary flooding have been examined. The main conclusions of the research may be summarised in the following points:

- Tri-sodium citrate dehydrate (SCD), was found to have non-negligible influences on the effective properties of brine, which were returned to approximately those of the plain synthetic brine by the addition of nanoparticles.
- Small concentrations provided higher enhancement of oil production at breakthrough, with a 20 ppm concentration providing an enhancement of 39.8% of OOIP compared to a value of 30.3% for water-flooding with plain synthetic brine. Whereas an oil recovery of only 31.8% of OOIP was achieved at breakthrough for 500 ppm.
- The best total cumulative recovery occurred for a 10 ppm nanofluid, with a total oil recovery of 41.8% of OOIP, representing a 38.0% increase on the plain water-flooding scenario.
- Post-breakthrough oil production was better for larger concentrations of nanoparticles. At the end of the flood, the 500 ppm nanofluid mobilised an additional 13.3 % of the original oil in place after breakthrough, which was partially attributed to a log-jamming effect.
- The concentration of particles trapped in the core after flooding increased with the increase of particle concentrations. Some of these nanoparticles could be removed from the core by subsequent flooding with plain synthetic brine, while some crossed into the oil phase, lowering its viscosity marginally.
- Different to the original mono particle size distribution, the effluent showed a bimodal distribution, and varied during the flood, which suggested that particles underwent a

complicated morphology change process during the core flooding.

- The wettability study shows that the water-wet Berea sandstone used in this work became progressively more water-wet by saturation with fluids of increasing nanoparticle concentrations.
- An analysis of the possible mechanisms for the enhanced oil recovery due to nanoparticles suggested that while the exact causes are unknown at present, the EOR effect in our experiments occurs through a combination of mobility ratio modification, rock wettability modification and log-jamming effect.

Further work is focusing on investigating the quantifiable relative permeability change introduced by nanoparticles, using a broader range of particles, rock types and nanoparticle concentrations, as well as quantifying the mechanisms leading to enhanced oil recovery through nanoEOR.

AUTHOR INFORMATION

Corresponding Author

*Phone: +44 (0)113 3431299, E-mail: d.wen@leeds.ac.uk

ACKNOWLEDGMENT

The work is supported by the European Research Council (ERC-2014-CoG, Project reference: 648375) and the China Scholarship Council (CSC).

References

1. Muggeridge, A.; Cockin, A.; Webb, K.; Frampton, H.; Collins, I.; Moulds, T.; Salino, P., Recovery rates, enhanced oil recovery and technological limits. *Philos. Trans. A Math. Phys. Eng. Sci.* **2012**, A372, 20120320.
2. Liu, F.; Guthrie, C. F.; Shipley, D., Optimizing Water Injection Rates for a Water-flooding Field In *SPE Ann. Tech. Conf.Exhibi.* Society of Petroleum Engineers: San Antonio, Texas, USA **2012**.
3. Skauge, T.; Spildo, K.; Skauge, A., Nano-sized Particles For EOR In *SPE Improved Oil Recov. Symp.* , Soc. Petrol. Eng. : Tulsa, USA, 2010.
4. Bayat, A. E.; Junin, R.; Samsuri, A.; Piroozian, A.; Hokmabadi, M., Impact of Metal Oxide Nanoparticles on Enhanced Oil Recovery from Limestone Media at Several Temperatures. *Energy Fuels* **2014**, 28, (10), 6255-6266.
5. Ayatollahi, S.; Zerafat, M. M., Nanotechnology-Assisted EOR Techniques: New Solutions to Old Challenges. In *SPE Int. Oilfield Nanotech. Conf. Exhibi.* , Society of Petroleum Engineers: Noordwijk, The Netherlands, **2012**.
6. Brinkman, H. C., The Viscosity of Concentrated Suspensions and Solutions. *J. Chem. Phys.* **1952**, 20, (4), 571.
7. Bobbo, S.; Fedele, L.; Benetti, A.; Colla, L.; Fabrizio, M.; Pagura, C.; Barison, S., Viscosity of water based SWCNH and TiO₂ nanofluids. *Exp. Therm. Fluid Sci.* **2012**, 36, 65-71.
8. Chen, H.; Ding, Y.; He, Y.; Tan, C., Rheological behaviour of ethylene glycol based titania nanofluids. *Chem. Phys. Lett.* **2007**, 444, (4-6), 333-337.
9. Roustaei, A.; Saffarzadeh, S.; Mohammadi, M., An evaluation of modified silica nanoparticles' efficiency in enhancing oil recovery of light and intermediate oil reservoirs. *Egypt. J. Petrol.* **2013**, 22, (3), 427-433.
10. Li, S.; Hendraningrat, L.; Torsater, O., Improved Oil Recovery by Hydrophilic Silica Nanoparticles Suspension: 2-Phase Flow Experimental Studies. In *Int.Petrol.Tech. Conf.* , Beijing, China, 2013.
11. Suresh, S., Studies on the dielectric properties of CdS nanoparticles. *Appl. Nanosci.* **2013**, 4, (3), 325-329.
12. Parvazdavani, M.; Masihi, M.; Ghazanfari, M. H., Monitoring the influence of dispersed nanoparticles on oil–water relative permeability hysteresis. *J. Petrol.Sci. Eng.* **2014**, 124, 222-231.
13. Karimi, A.; Fakhroueian, Z.; Bahramian, A.; Pour Khiabani, N.; Darabad, J. B.; Azin, R.; Arya, S., Wettability Alteration in Carbonates using Zirconium Oxide Nanofluids: EOR Implications. *Energy Fuels* **2012**, 26, (2), 1028-1036.
14. Hwang, C.-C.; Wang, L.; Lu, W.; Ruan, G.; Kini, G. C.; Xiang, C.; Samuel, E. L. G.; Shi, W.; Kan, A. T.; Wong, M. S.; Tomson, M. B.; Tour, J. M., Highly stable carbon nanoparticles designed for downhole hydrocarbon detection. *Energ. Env. Sci.* **2012**, 5, (8), 8304.
15. Hwang, C. C.; Ruan, G.; Wang, L.; Zheng, H.; Samuel, E. L.; Xiang, C.; Lu, W.; Kasper, W.; Huang, K.; Peng, Z.; Schaefer, Z.; Kan, A. T.; Marti, A. A.; Wong, M. S.; Tomson, M. B.; Tour, J. M., Carbon-based nanoreporters designed for subsurface hydrogen sulfide detection. *ACS Appl. Mat. Interf.* **2014**, 6, (10), 7652-7658.
16. Alaskar, M. In-Situ Multifunctional Nanosensors for Fractured Reservoir Characterization. Stanford University , Stanford, California, **2013**.
17. Ehtesabi, H.; Ahadian, M. M.; Taghikhani, V.; Ghazanfari, M. H., Enhanced Heavy Oil Recovery in Sandstone Cores Using TiO₂Nanofluids. *Energy Fuels* **2014**, 28, (1), 423-430.
18. Singh, R.; Mohanty, K. K., Synergy between Nanoparticles and Surfactants in Stabilizing Foams for Oil Recovery. *Energy Fuels* **2014**, 29, (2), 467-479.

19. Pei, H. H.; Zhang, G. C.; Ge, J. J.; Zhang, J.; Zhang, Q.; Fu, L. P., Investigation of Nanoparticle and Surfactant Stabilized Emulsion to Enhance Oil Recovery in Waterflooded Heavy Oil Reservoirs In *SPE Canada Heavy Oil Tech. Conf.*, Soc. Petrol. Eng. : Calgary, Alberta, **2015**.
20. Suleimanov, B. A.; Ismailov, F. S.; Veliyev, E. F., Nanofluid for enhanced oil recovery. *J. Petrol. Sci. Eng.* **2011**, 78, (2), 431-437.
21. Hendraningrat, L.; Li, S.; Torsæter, O., A coreflood investigation of nanofluid enhanced oil recovery. *J. Petrol. Sci. Eng.* **2013**, 111, 128-138.
22. Wang, Y.; Becker, M. D.; Colvin, V. L.; Abriola, L. M.; Pennell, K. D., Influence of residual polymer on nanoparticle deposition in porous media. *Environ. Sci. Technol.* **2014**, 48, (18), 10664-10671.
23. Fan, W.; Jiang, X.; Lu, Y.; Huo, M.; Lin, S.; Geng, Z., Effects of surfactants on graphene oxide nanoparticles transport in saturated porous media. *J. Environ. Sci.* **2015**, 35, 12-19.
24. Alagic, E.; Spildo, K.; Skauge, A.; Solbakken, J., Effect of crude oil ageing on low salinity and low salinity surfactant flooding. *J. Petrol. Sci. Eng.* **2011**, 78, (2), 220-227.
25. Spildo, K.; Sun, L.; Djurhuus, K.; Skauge, A., A strategy for low cost, effective surfactant injection. *J. Petrol. Sci. Eng.* **2014**, 117, 8-14.
26. Revil, A.; Glover, P. W. J., Theory of ionic-surface electrical conduction in porous media. *Phys. Rev. B* **1997**, 55, (3), 1757-1773.
27. Revil, A.; Glover, P. W. J., Nature of surface electrical conductivity in natural sands, sandstones, and clays. *Geophysical Res. Lett.* **1998**, 25, (5), 691-694.
28. Glover, P. W. J., Geophysical Properties of the Near Surface Earth: Electrical Properties. In *Treatise on Geophysics*, Schubert, G. (Editor-in-chief), Elsevier: Oxford, 2015; Vol. 11, pp 89-137.
29. Wen, DS, Corr, M. Hu,X and Lin G: Boiling heat transfer of nanofluids: the effect of heating surface modification. *Int. J. Therm. Sci.* , **2011**, 50, 480-485
30. Caputo, G.; Nobile, C.; Kipp, T.; Blasi, L.; Grillo, V.; Carlino, E.; Manna, L.; Cingolani, R.; Cozzoli, P. D.; Athanassiou, A., Reversible Wettability Changes in Colloidal TiO₂ Nanorod Thin-Film Coatings under Selective UV Laser Irradiation. *J. Phys. Chem. C* **2008**, 112, 701-714.
31. Vafei, S and Wen, DS. Bubble formation on a submerged micronozzle. *J. Coll. Interf. Sci.* , **2010**, 343, 291-297.
32. Vafei, S and Wen, DS. Critical heat flux (CHF) of subcooled flow boiling of alumina nanofluids in a horizontal microchannel. *J. Heat Transfer - Trans. of ASME.* **2010**,132, 102404
33. Venerus, David C.; Buongiorno, Jacopo; Christianson, Rebecca; et al. iscosity measurements on colloidal dispersions (nanofluids) for heat transfer applications. *Appl.Rheology*, **2010**,20, 44582
34. Zhu, D.; Han, Y.; Zhang, J.; Li, X.; Feng, Y., Enhancing rheological properties of hydrophobically associative polyacrylamide aqueous solutions by hybridizing with silica nanoparticles. *J. Appl. Polym. Sci.* **2014**, 131, (19), 40876.
35. Wasan, D. T.; Nikolov, A. D., Spreading of nanofluids on solids. *Nature* **2003**, 423, 156-159.
36. Nikolov, A.; Wasan, D., Wetting-dewetting films: the role of structural forces. *Adv. Colloid. Inter. Sci.* **2014**, 206, 207-21.
37. Shahrabad, A.; Bagherzadeh, H.; Roustaei, A.; Golghanddashti, H., Experimental investigation of HLP nanofluid potential to enhanced oil recovery. In *SPE Int. Oil Field Nanotech. Conf.* , Noordwijk, Netherlands, **2012**.
38. Hendraningrat, L.; Shidong, L.; Torsater, S. a. O., A Glass micromodel experimental study of hydrophilic nanoparticles retention for eor project. In *SPE Russian Oil & Gas Explor. & Prod. Tech. Conf. Exhib.* Moscow, Russia, **2015**.
39. El-Diasty, A. I.; Aly, A. M., Understanding the Mechanism of Nanoparticles Applications in Enhanced Oil Recovery. In *SPE North Africa Technical Conference and Exhibition*, Soc. Petrol. Eng. : Cairo, Egypt **2015**.

40. Wen, D.S., On the role of structural disjoining pressure to boiling heat transfer with thermal nanofluids. *J. Nanopar. Res.* **2008**, 10, (7), 1129-1140.
41. Wang, Y.; Li, Y.; Fortner, J. D.; Hughes, J. B.; Abriola, L. M.; Pennell, K. D., Transport and Retention of Nanoscale C60 Aggregates in Water-Saturated Porous Media. *Environ. Sci. Technol* **2008**, 42, (10), 3588–3594.
42. Shani, C.; Weisbrod, N.; Yakirevich, A., Colloid transport through saturated sand columns: Influence of physical and chemical surface properties on deposition. *Colloid. Surf. A: Physicochem. Eng. Asp.* **2008**, 316, (1-3), 142-150.
43. Yoon, J. S.; Germaine, J. T.; Culligan, P. J., Visualization of particle behavior within a porous medium: Mechanisms for particle filtration and retardation during downward transport. *Water Resour. Res.* **2006**, 42, (6), W06417.
44. Wang, C.; Bobba, A. D.; Attinti, R.; Shen, C.; Lazouskaya, V.; Wang, L. P.; Jin, Y., Retention and transport of silica nanoparticles in saturated porous media: effect of concentration and particle size. *Environ. Sci. Technol.* **2012**, 46, (13), 7151-7158.
45. Hendraningrat, L.; Torsæter, O., Metal oxide-based nanoparticles: revealing their potential to enhance oil recovery in different wettability systems. *Appl. Nanosci.* **2014**, 5, (2), 181-199.
46. Zhulina, E. B.; Borisov, O. V.; Priamitsyn, V. A., Theory of Steric Stabilization of Colloid Dispersions by Grafted Polymers. *J. Colloid. Interf. Sci.* **1990**, 137, (2), 495-511.
47. Fritz, G.; Schadler, V.; Willenbacher, N.; Wagner, N. J., Electrosteric Stabilization of Colloidal Dispersions. *Langmuir* **2002**, 18, (16), 6381-6390.
48. Metin, C. O.; Lake, L. W.; Miranda, C. R.; Nguyen, Q. P., Stability of aqueous silica nanoparticle dispersions. *J. Nanopar. Res.* **2011**, 13, (2), 839-850.
49. Agarwal, D. K.; Vaidyanathan, A.; Sunil Kumar, S., Synthesis and characterization of kerosene–alumina nanofluids. *Appl. Therm. Eng.* **2013**, 60, (1-2), 275-284.
50. French, R. A.; Jacobson, A. R.; Kim, B.; Isley, S. L.; Penn, R. L.; Baveye, P. C., Influence of ionic strength, pH, and cation valence on aggregation kinetics of titanium dioxide nanoparticles. *Environ. Sci. Technol.* **2009**, 43, (5), 1354-1359.
51. Solovitch, N.; Labille, J.; Rose, J.; Chaurand, P.; Borschneck, D.; Wiesner, M. R.; Bottero, J. Y., Concurrent aggregation and deposition of TiO₂ nanoparticles in a sandy porous media. *Environ. Sci. Technol.* **2010**, 44, (13), 4897-902.
52. Bouhaik, I. S.; Leroy, P.; Ollivier, P.; Azaroual, M.; Mercury, L., Influence of surface conductivity on the apparent zeta potential of TiO₂ nanoparticles: Application to the modeling of their aggregation kinetics. *J. Colloid Interf. Sci.* **2013**, 406, 75-85.
53. Glover, P. W. J.; Dery, N., Streaming potential coupling coefficient of quartz glass bead packs: Dependence on grain diameter, pore size, and pore throat radius. *Geophysics* **2010**, 75, (6), F225-F241.
54. Pieranski, P., Two-Dimensional Interfacial Colloidal Crystals. *Phys. Rev. Lett.* **1980**, 45, (7), 569-572.
55. Du, K.; Glogowski, E.; Emrick, T.; Russell, T. P.; Dinsmore, A. D., Adsorption energy of nano- and microparticles at liquid-liquid interfaces. *Langmuir*; **2010**, 26, (15), 12518-12522.
56. Du, K.; Liddle, J. A.; Berglund, A. J., Three-dimensional real-time tracking of nanoparticles at an oil-water interface. *Langmuir* **2012**, 28, (25), 9181-9188.
57. Vinogradov, J.; Jackson, M. D., Zeta potential in intact natural sandstones at elevated temperatures. *Geophys. Res. Lett.* **2015**, 42, 6287-6294.
58. Walker, E.; Glover, P. W. J.; Ruel, J., A transient method for measuring the DC streaming potential coefficient of porous and fractured rocks. *J. Geophys. Res.-Sol. Ea* **2014**, 119, (2), 957-970.
59. Glover, P.; Walker, E.; Jackson, M., Streaming-potential coefficient of reservoir rock: A theoretical model. *Geophysics* **2011**, 77, 17-43

60. Becker, M. D.; Wang, Y.; Pennell, K. D.; Abriola, L. M., A multi-constituent site blocking model for nanoparticle and stabilizing agent transport in porous media. *Environ. Sci.: Nano* **2015**, 2, (2), 155-166.
61. Glover, P. W. J., A generalized Archie's law for n phases. *Geophysics* **2010**, 75, (6), E247-E265.
62. Kumar, M.; Hoang, V. T.; Satik, C.; Rojas, D. H., High-Mobility-Ratio Waterflood Performance Prediction: Challenges and New Insights. *SPE Reserv. Evalu. Eng.* **2013**, 11, (01), 186-196.
63. Shahrabadi, A.; Bagherzadeh, H.; Roostaie, A.; Golghanddashti, H., Experimental Investigation of HLP Nanofluid Potential to Enhance Oil Recovery: A Mechanistic Approach, In *SPE Int. Oilfield Nanotech. Conf. Exhib.* Soc. Petrol. Eng. : Noordwijk, The Netherlands **2012**.
64. Vafaei, S. and Wen, DS, Bubble formation in a quiescent pool of gold nanoparticle suspension. *Adv. Coll. Interf. Sci.* , **2010**, 159, (10), 72-93.
65. Kim, S. J.; Bang, I. C.; Buongiorno, J.; Hu, L. W., Surface wettability change during pool boiling of nanofluids and its effect on critical heat flux. *Int. J. Heat Mass Trans.* **2007**, 50, (19-20), 4105-4116.
66. Kim, S. J.; Bang I. C.; Buongiorno J.; Hu, L. W., Study of pool boiling and critical heat flux enhancement in nanofluids. *Bull. Polish. Acad. Sci. Tech. Sci.* **2007**, 55, 211-216.
67. Sethumadhavan, G. N.; Nikolov, A. D.; Wasan, D. T., Stability of Liquid Films Containing Monodisperse Colloidal Particles. *J. Colloid. Interf. Sci.* **2001**, 240, (1), 105-112.
68. Kondiparty, K.; Nikolov, A.; Wu, S.; Wasan, D., Wetting and spreading of nanofluids on solid surfaces driven by the structural disjoining pressure: statics analysis and experiments. *Langmuir* **2011**, 27, (7), 3324-3335.
69. Chengara, A.; Nikolov, A. D.; Wasan, D. T.; Trokhymchuk, A.; Henderson, D., Spreading of nanofluids driven by the structural disjoining pressure gradient. *J. Colloid. Interf. Sci.* **2004**, 280, (1), 192-201.
70. Kondiparty, K.; Nikolov, A. D.; Wasan, D.; Liu, K. L., Dynamic spreading of nanofluids on solids. Part I: experimental. *Langmuir* **2012**, 28, (41), 14618-14623.
71. Wasan, D.; Nikolov, A.; Kondiparty, K., The wetting and spreading of nanofluids on solids: Role of the structural disjoining pressure. *Curr. Opin. Colloid Interf. Sci.* **2011**, 16, (4), 344-349.
72. Zhang, H.; Nikolov, A.; Wasan, D., Dewetting film dynamics inside a capillary using a micellar nanofluid. *Langmuir* **2014**, 30, (31), 9430-9435.
73. Onyekonwu, M. O.; Ogolo, N. A., Investigating the use of nanoparticles in enhanced oil recovery. In *Nigeria Ann. Int. Conf. Exhibit.* , Soc. Petrol. Eng. : Tinapa - Calabar, Nigeria, **2010**.